OMOCLO README FILE
Date of this Document: 1 May 2008

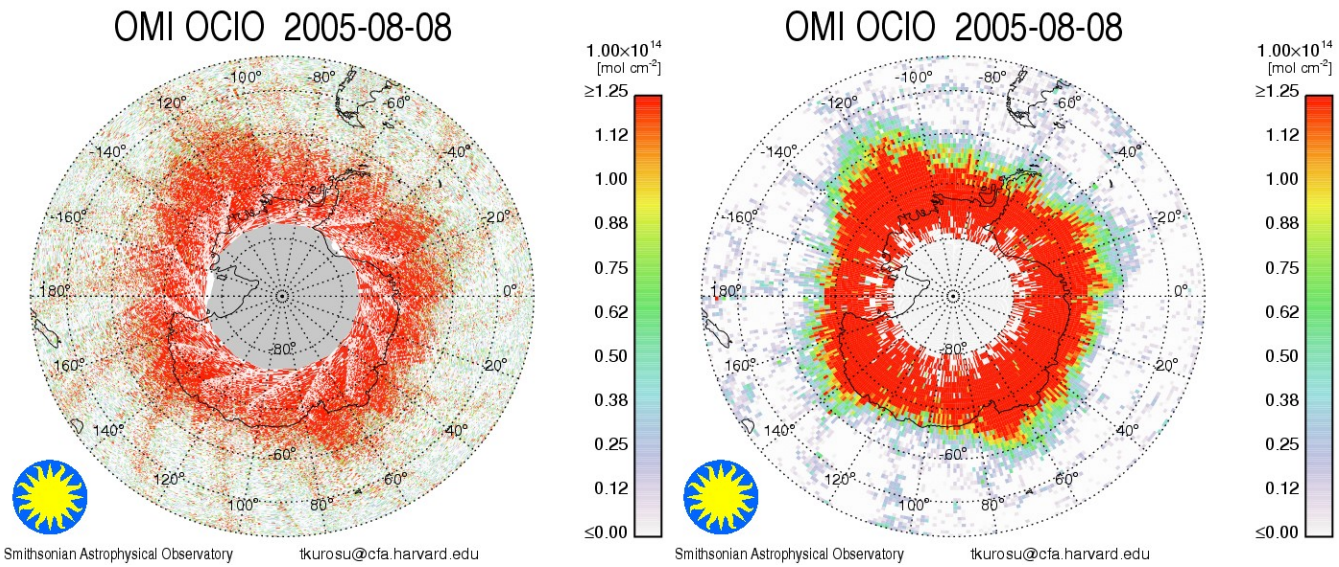

Overview

This document provides a brief description of the OMOCLO data product. OMOCLO contains slant column OClO and ancillary information retrieved from OMI global and spatial zoom mode measurements using a retrieval algorithm that is based on non-linear least-squares fitting originally developed for GOME, and adapted for the OMI instrument. In global mode, *i.e.*, global coverage in one day, each file contains a single orbit of data covering a swath of approximately 2,600 km wide from pole to pole (sunlit portions only).

Fitting uncertainties for the OClO slant columns (single measurement) typically range between 40-100%, with the lower end of this range within the Antarctic polar vortex where OClO is most abundant.

The images above shows OClO on 8 August 2005: The plot on the left shows the fitted slant columns from the 15 individual orbits of that day; the plot on the right contains the same data but averaged onto a grid of resolution 1°x1° (latitude x longitude).

Release History and Release-Specific Information

OMOCLO Algorithm Version[1]	2.0
Collection/Product Version[1]	003
This Public Release	1 May 2008
First Public Release	1 February 2007
Validation Release	25 December 2005
Known Issue List	Across-track striping in the data product

1 *Algorithm Version* (level-2 related) and *Collection/Product Version* (level-1 related) must not be confused: While the Collection/Product Version number is part of any OMOCLO data file name, *e.g.*,
`OMI-Aura-L2-OMOCLO_<acquisition date>-o<orbit number>_v003-<processing date>.he5`
the Algorithm Version is stored within the data product file, in the Metadata field PGEVERSION.

Algorithm Description

The algorithm is based on the direct fitting of radiances and irradiances. In particular, and differing from what is commonly referred to as Differential Optical Absorption Spectroscopy (DOAS) fitting, radiances are not divided by irradiances, no logarithms are taken of the spectra, and no high-pass filtering is applied. In the current version, an OMI radiance measurement from the same granule is used in lieu of an irradiance measurement.

The four main stages of the algorithm are (1) Solar wavelength calibration, in which the optimum wavelength registration of the composite solar irradiance, derived from a principal component analysis of three years of individual OMI irradiance measurements, is determined; (2) Radiance wavelength calibration, which finds the optimum wavelength registration for a representative swath of radiance measurements (usually in the middle of the orbit) and determines a common wavelength grid for auxiliary data bases (molecular reference cross sections, *etc*.); (3) On-line computation of a residual "common mode" spectrum; and (4) Non-linear, least-squares fitting of all swath lines in the OMI granule. In each stage, the calibration/fitting is performed individually for the 60 cross-track pixels[2] of an OMI swath line. For improved numerical stability, radiances and irradiances are divided by their respective averages over the fitting window; in other words, they are "normalized" to values ~1.

OClO fitting is performed in the spectral window 358.5.5–392.0nm, within the VIS channel of the OMI instrument. The model that is fitted to the measurements consists of the radiance reference (from the remote Pacific), attenuated by contributions from OClO (the target gas), inelastic (rotational Raman, or *Ring*) scattering, and interferences from from other atmospheric gases, including NO_2, BrO, and O_3; it also contains additive and multiplicative closure polynomials and parameters for spectral shift and, potentially, squeeze, as well as a sampling correction [Chance *et al*., 2005] and a common mode spectrum, both of which are computed on-line. The common mode spectra (one per cross-track position) are the average of several hundred fitting residuals and include any instrument effects that are unrelated to molecular scattering and absorption cross sections. The least-squares fit is mostly unconstrained, with the exception of selected parameters, including the spectral shift, which are constrained in order to prevent problems arising from out-of-bounds values.

The results from the spectral fitting are OClO slant columns. No conversion to vertical column is performed since OClO is currently detectable only inside the polar vortex during the Arctic and Antarctic Spring and hence associated with large solar zenith angles, close to or exceeding 90°

The algorithm employs several methods to reduce cross-track striping of the OClO columns. These include "soft calibration" (*i.e*., the use of a radiance reference), outlier screening in the fitting residuals, the use of a composite solar spectrum (all employed during the fitting process), as well as a post-processing cross-track smoothing of the fitted columns. These smoothed columns are provided in a separate data field, *ColumnAmountDestriped*. In the current version the smoothed columns are included more for historic reasons, since advances in level-1 radiance calibration, particularly the time-dependent OPF, and the OClO retrievals themselves have brought the regular columns to a level where further destriping is of little benefit. It must also be pointed out that the across-track smoothing almost certainly introduces an as yet unquantified bias to the fitted columns. For the present version, the use of *ColumnAmountDestriped* is discouraged.

More details on algorithm specifics can be found in the OMI Algorithm Theoretical Basis Document Vol. 4, and in Kurosu *et al*. [2004]. A summary table of algorithm specifics and molecular cross-section data bases used in the fitting is provided at the end of this document.

Data Quality Assessment

Across-track striping (systematically elevated or reduced column values at the same cross track position along the whole track) of the OClO columns is still an issue, despite the improvements achieved in OMOCLO v2.0 (Collection/Product Version 003). This is not unique to OClO but affects all OMI data products to a greater or lesser extent. Small absorbers like BrO, HCHO and OClO however, are more strongly affected by striping since the column values are of a similar order of magnitude as the stripes, so that the effect is relatively stronger. Users of the OClO columns provided here must be aware of this issue.

The OClO data product provides RMS (data field *FittingRMS*) and one standard deviation (1σ) fitting uncertainties (*ColumnUncertainty*), as derived from the fitting covariance matrix. The uncertainties do not include contributions from uncertainties in the measurements or the reference cross sections. The main guidance to data quality

2 Alternatively: 30 cross-track pixels in rebinned spatial zoom mode, occurring every 32 days.

provided with the OClO columns is the *MainDataQualityFlag*, which is set to any of four values (0, 1, 2, and -1) based on the outcome of the fitting process (see description below, under "Which Data Should Be Used?"). This flag should be used for data screening prior to use of each individual OMI pixel column. Additional information on the convergence of the fit is provided in a fitting diagnostic flag (*FitConvergenceFlag*); this flag should be consulted if more detailed information on the fitting process is desired. For details see the product specification document OMOCLO.fs or consult the File Specification README.

Cloud Information

Clouds are not considered in the OMOCLO retrievals.

Preliminary Validation

Due to very limited amount of correlative OClO measurements, only few validation activities for the OMI OClO product are currently ongoing. These mainly consist of comparisons with two other satellite instruments, GOME and SCIAMACHY. At present, only very preliminary results from satellite comparisons are available.

Direct comparisons with GOME data products are difficult since OClO retrievals from GOME are no longer reliable due to the advanced degradation of the GOME instrument. First comparisons with SCIAMACHY OClO data during the Antarctic polar vortex (August 2005) show that OMI OClO captures the distribution within the vortex, and slant column values compare well with SCIAMACHY.

Which Data Should Be Used?

Each SAO data product (BrO, HCHO, OClO) contains the data field *MainDataQualityFlag* to aid the user in the selection of which data to use and which to avoid. Each ground pixel is assigned a value, the range and classification of which are as follows:

Value	Classification	Rationale
0	Good	Column value present and passes all quality checks; data may be used with confidence.
1	Suspect	Caution advised because one or more of the following conditions are present: • *FitConvergenceFlag* is < 300 (but > 0): convergence at noise level • Column+2σ uncertainty < 0 (but Column+3σ uncertainty ≥ 0) • Absolute column value > *MaximumColumnAmount* ($1 \bullet 10^{19}$ mol/cm^2)
2	Bad	Avoid using data because one or more of the following conditions are present: • *FitConvergenceFlag* is < 0: abnormal termination, no convergence • Column+3σ uncertainty < 0
≤ -1	Missing	No column values have been computed; entries are missing

Product Description

A 2600 km wide OMI swath contains 60 cross-track pixels, ranging in size from 14x24 km^2 (along x across track) in the center of the swath to about 28x150 km^2 at the edges of the swath (median: 15x33 km^2). The pixels on the swath are not symmetrically aligned on the line perpendicular to the orbital plane. However, the latitude and longitude provided with each pixel represents the location of each pixel on the ground to a fraction of a pixel.

The OMOCLO product is written as HDF-EOS5 swath file. A single OMOCLO file contains information retrieved from each OMI pixel over the sun-lit portion of the orbit (a.k.a. an *OMI granule*). The information provided in these files include: Geodetic longitude and latitude, solar and line-of-sight zenith and azimuth angles, slant column OClO with RMS and 1σ fitting uncertainties, longitude and latitude corner coordinates for each OMI pixel, and a range of ancillary parameters that provide information to assess data quality. Average values over an OMI granule for the OClO total column, uncertainties, and RMS, as well as the percent values of "good" (converged and columns positive within 2σ fitting uncertainties) and "bad" (failed convergence or truly negative columns)

provide general, granule-based information on data quality. For a complete list of data fields and their description, please read the file specifications OMOCLO.fs or see the File Specification README.

OMOCLO data are publicly available from NASA's OMI/Aura Data Products Web Page (GES-DISC). Also, subsets of these data over many ground stations and along Aura validation aircraft flight paths are available through the Aura Validation Data Center (AVDC) website to those investigators who are associated with the various Aura science teams.

For questions and comments related to the OMOCLO dataset please contact Raid M. Suleiman. Please send a copy of your e-mail to Kelly Chance, who has the overall responsibility for this product.

Summary of Algorithm Fitting Specifics

Fitting window	358.5 – 392.0 nm
Baseline polynomial	2nd order
Scaling polynomial	3rd order
Instrument slit function	Hyper-parameterization of pre-flight measurements
Wavelength calibration	Spectral shift (no squeeze)
Solar reference spectrum	Kurucz, 1995
O_3 cross sections	Malicet *et al*., 1995; 228K
NO_2 cross sections	Vandaele *et al*., 1998; 220K
BrO cross section	Wilmouth *et al.*, 1999; 228K
OClO cross sections	Kromminga et al., 1999; 213K
O_2-O_2 cross sections	Hermans (BISA); 294K
Molecular Ring cross sections	Chance and Spurr, 1997
Vibrational Raman ("Water Ring") cross sections	Chance and Spurr, 1997
Sampling correction	Computed on-line
Residual common mode spectrum	Computed on-line

Selected List of Elements in an OMOCLO Output File

The tables below show a selected list of data elements in an OMOCLO HDF-EOS5 output file. The tables are divided into (*a) Swath Dimensions*, *(b) Geolocation Fields*, and *(c) Data Fields*. The selection of the listed *Geolocation* and *Data Field*s is entirely arbitrary and made solely to facilitate the identification of what is assumed will be the most-used parameters from the OMOCLO data product. No such distinction is made in the HDF-EOS5 product file itself. Naturally, whether or not any part of the product is of interest ultimately depends on the application. For a complete list of fields please refer to OMSAO_FileSpecifications_README.pdf.

(a) Swath Dimensions

Field Name	Field Type	Description
nTimes	HE5T_NATIVE_INT	Number of swath lines in an OMI granule (usually about 1650)
nXtrack	HE5T_NATIVE_INT	Number of cross-track positions in a swath line (usually 30 or 60)
nUTCdim	HE5T_NATIVE_INT	Number of elements in a single *TimeUTC* field entry (6)

(b) Geolocation Fields of prime interest

Field Name	Field Type	Dimensions	Description
Latitude	HE5T_NATIVE_FLOAT	nXtrack,nTimes	Geodetic latitude [deg] at the center of the ground pixel
Longitude	HE5T_NATIVE_FLOAT	nXtrack,nTimes	Geodetic longitude [deg] at the center of the ground pixel
SolarZenithAngle		nXtrack,nTimes	The solar zenith angle [deg] at the center of the ground pixel
TimeUTC	HE5T_NATIVE_INT16	nUTCdim,nTimes	UTC value of the TAI93 time. The 6 different elements of the UTC string `YYYY-MM-DD hh:mm` are stored in the 6 arrays positions.
ViewingZenithAngle	HE5T_NATIVE_FLOAT	nXtrack,nTimes	The viewing zenith angle [deg] at the center of the ground pixel

(c) Data Fields of prime interest

Field Name	Field Type	Dimensions	Description
ColumnAmount	HE5T_NATIVE_DOUBLE	nXtrack,nTimes	Slant column amount [mol/cm^2] for each ground pixel
ColumnUncertainty	HE5T_NATIVE_DOUBLE	nXtrack,nTimes	Slant column amount uncertainty [mol/cm^2] for each ground pixel
MainDataQualityFlag	HE5T_NATIVE_INT16	nXtrack,nTimes	Main flag to indicate data quality (see above)
PixelCornerLatitudes	HE5T_NATIVE_FLOAT	nXtrack+1,nTimes+1	The geodetic latitudes [deg] of the corner coordinates of the OMI ground pixels.
PixelCornerLongitudes	HE5T_NATIVE_FLOAT	nXtrack+1,nTimes+1	The geodetic longitudes [deg] of the corner coordinates of the OMI ground pixels.

References

OMI Algorithm Theoretical Basis Document, Volume IV, OMI Trace Gas Algorithms, OMI-ATBD-VOL4, ATBD-OMI-04, Version 2.0, August 2002.

Cantrell, C.A., J.A. Davidson, A.H. McDaniel, R.E. Shetter, and J.G. Calvert, Temperature-dependent formaldehyde cross-sections in the near-ultraviolet spectral region, *Journal of Physical Chemistry*, 94, pp 3902-3908 (1990)

Chance, K, and R.J.D. Spurr, Ring effect studies: Rayleigh scattering, including molecular parameters for rotational Raman scattering, and the Fraunhofer spectrum, *Applied Optics*, 36, pp 5224-5230 (1997)

Chance, K., T.P. Kurosu, and C.E. Sioris, Undersampling correction for array-detector based satellite spectrometers, Applied Optics 44(7), 1296-1304 (2005).

Hermans, C., http://www.oma.be/BIRA-IASB/Scientific/Topics/Lower/LaboBase/Laboratory.html

Kromminga, H., S. Voigt, J. Orphal, and J.P. Burrows, UV-Visible FT Spectra of OClO at Atmospheric Temperatures, *Proceedings of the 1st European Symposium on Atmospheric Measurements from Space*, ESA Special Publication (1999)

Kurosu, T.P., K. Chance, and C.E. Sioris, "Preliminary results for HCHO and BrO from the EOS-Aura Ozone Monitoring Instrument", in *Passive Optical Remote Sensing of the Atmosphere and Clouds IV, Proc. of SPIE Vol. 5652*, doi: 10.1117/12.578606 (2004).

Kurucz, R.L., The Solar Spectrum: Atlases and Line Identifications, in *Laboratory and Astronomical High Resolution Spectra*, A. Sauval, R. Blomme, and N. Grevesse, Eds., 81, pp 17-31, Astronomical Society of the Pacific Conference (1995)

Malicet, J., D. Daumont, J. Charbonnier, C. Parisse, A. Chakir, and J. Brion, Ozone UV spectroscopy. II. Absorption cross-sections and temperature dependence, *Journal of Atmospheric Chemistry*, 21 (3), pp 263-273 (1995)

Vandaele A.C., C. Hermans, P.C. Simon, M. Carleer, R. Colin, S. Fally, M.F. Mérienne, A. Jenouvrier, and B. Coquart, Measurements of the NO_2 absorption cross-section from 42000 cm^{-1} to 10000 cm^{-1} (238-1000 nm) at 220 K and 294 K, *Journal of Quantitative Spectroscopy and Radiative Transfer*, 59, pp 171-184 (1998)

Wilmouth, D.M., T.F. Hanisco, N.M. Donahue, and J.G. Anderson, Fourtier transform ultraviolet spectroscopy of the $A^2\,\Pi_{3/2} \rightarrow X^2\,\Pi_{3/2}$ transition of BrO, J*ournal of Physical Chemistry A*, 103, pp 8935-8945 (1999)